Lecture Notes in Engineering

Edited by C. A. Brebbia and S. A. Orszag

54

T. J. Mueller (Editor)

Low Reynolds Number Aerodynamics

Proceedings of the Conference
Notre Dame, Indiana, USA, 5–7 June 1989

Springer-Verlag

Low Reynolds Number Airfoil Design and Wind Tunnel Testing at Princeton University

J. F. Donovan† & M. S. Selig‡

Princeton University
Gas Dynamics Laboratory
Princeton, NJ 08544

Abstract

This paper focuses on the development of efficient low Reynolds number airfoils. Both experimental and computational techniques were used. The experimental facility and measurement technique are discussed in detail, and turbulence measurements in the tunnel freestream are presented. Lift and Drag data were taken at chord Reynolds numbers between 0.6×10^5 and 3.0×10^5. Comparisons of data obtained in the Princeton facility with that in several others are presented and show good agreement. Based on the results of over 40 airfoils tested during the first phase of this program (including the DAE51, FX63-137, E205, E374, E214, E387, Miley, NACA 0009, S3021, S2091, S4233), several new airfoils were designed using the Eppler and Somers code and screened using the Drela and Giles ISES code. Seventeen of the most promising designs were actually wind tunnel tested. The design philosophy is discussed and verified experimentally. Several of the new airfoils show significant performance improvements over previous airfoils. Boundary layer trips were also investigated as a means of reducing drag. Several types of trips were compared (zig-zag trips, bump tape, blowing, and two-dimensional trips), and the simple two-dimensional trip was found to yield the greatest improvement. The effects of model inaccuracies are also discussed, as well as the importance of a thin trailing edge in achieving low drag.

1. Introduction

The distinguishing characteristic of an airfoil operated at low chord Reynolds numbers ($Re < 5.0 \times 10^5$) is the formation of an extensive laminar separation bubble on either the upper or lower surface or both. This bubble can significantly increase the drag. As the laminar boundary layer negotiates the adverse pressure gradient of recovery it separates, thereby defining the beginning of the bubble. Amplified by the adverse pressure gradient, instabilities in the resulting free shear layer cause it to become turbulent. In most cases, the enhanced momentum transfer provided by the turbulent free shear layer allows it to reattach. Laminar separation bubbles not only increase airfoil drag but also cause hysteresis in both lift and drag with angle of attack.

In the past, developing methods of dealing with laminar separation bubbles to reduce drag has received little attention. Recently, however, a growing need for efficient

† Research Scientist, McDonnell Douglas Research Laboratories, P. O. Box 516, St Louis, MO 63166

‡ Graduate Student, The Pennsylvania State University, 233 Hammond Bldg., University Park, PA 16802

low Reynolds number airfoils has prompted interest in this area. Much of the experimental and theoretical effort has been concentrated on a fundamental understanding of laminar separation bubbles[1,2] in the hopes of predicting their behavior. This type of investigation has not yet led to the accurate prediction of low Reynolds number airfoil performance, and thus, the design problem still remains. However, efficient designs can be developed based on a limited knowledge of laminar separation bubble behavior.

Performance may be improved by reducing the size of the laminar separation bubble through the use of (1) transition ramps[3] (or more appropriately called a "bubble ramp") or (2) boundary layer trips[1]. Presently it is unclear if the optimum airfoil for a given task would make use of either or both of these techniques. Moreover, little data exists on the effects of boundary layer trips on low Reynolds number airfoil performance.

The approach of this investigation was to evaluate existing airfoil designs as well as the effects of trips on their performance, and then, based upon this limited information, to design more efficient airfoils. These new airfoils were developed through the use of the Eppler and Somers code[4] and the Drela and Giles ISES[5,6] code. In all, 62 airfoil sections were tested (17 of which were new designs) under various conditions resulting in 130 polars. Measurements were generally taken at Reynolds numbers of 0.6×10^5, 1.0×10^5, 1.5×10^5, $2.0 \times 10^5$and 3.0×10^5.

An important concern when taking measurements at low Reynolds numbers is the high sensitivity of the flow to freestream disturbances. A high freestream turbulence level can cause transition to occur sooner in the free shear layer and, as a result, reduce drag. In this investigation, the freestream turbulence properties have been well documented.

This paper is broken into two major sections. First, the experimental facility and measurement technique are discussed. Second, some important highlights of these experiments are presented, and finally, several conclusions are drawn. Further details and a complete compilation of this data (including the over 130 polars as well as the tabulated data) may be found in Reference 7.

2. Experimental Facility and Measurement Technique

The tests were performed in the Princeton University 3 ft by 4 ft Smoke Tunnel. A sketch of the tunnel is shown in Figure 1. It consists of an inlet and stilling chamber 9 ft high by 12 ft wide containing screens and flow straighteners. The flow straighteners are 3 in square and 12 in long. This section is followed by a 9:1 contraction leading to the test section 4 ft wide by 3 ft high. Downstream of the test section the flow is turned by 90° and exits through a 50 HP fan. The tunnel speed in the test section was variable from 5 ft/s to 70 ft/s.

2.1 Flow Quality

Constant-temperature hot-wire anemometry[8] (using Dantec model 55M01) was used to determine turbulence levels in the freestream. At all conditions, the wire was operated at an overheat of 0.8. Frequency response was optimized using the standard square-wave test in which a square wave voltage is injected at the Wheatstone bridge to simulate an impulse in velocity. The -3 dB point of the response curve was at 33 kHz for chord Reynolds numbers of 1.0×10^5, 2.0×10^5, and 3.0×10^5, and at 25 kHz for a

Reynolds number of 0.6 $\times 10^5$. These frequencies are well above the energy containing frequencies as will be shown shortly.

A common problem when measuring turbulence levels in low-speed facilities is determining the lowest frequency of interest. Usually, the anemometer signal is high-pass filtered, leaving only the fluctuating component. This technique removes possibly important contributions of low frequency turbulent fluctuations to the RMS. In this work, however, no high-pass filter was used. Instead, the DC component (the mean) of the anemometer signal was subtracted off ("bucked off") using an OP-amp summer of an analog computer. The remaining signal was then amplified to fill the range of the A/D converter and sampled at frequencies from 10 Hz to 10 kHz. By sampling over a range of frequencies, high resolution of the spectra was obtained. In each case the low-pass frequency of the filter was set to a frequency somewhat less than the Nyquist sampling frequency to eliminate alaising errors.

An example spectrum is shown in Figure 2 for a Re of 1.0 $\times 10^5$. Power spectral density multiplied by frequency is plotted against the logarithm of frequency. In this way, the area under the curve is directly proportional to $(u'_{rms})^2$. The sampling frequency was 100 Hz, and the hot wire was located along the tunnel horizontal centerline and 3 in below the vertical centerline. In this case the turbulence level, u'_{rms}/U_∞, is 0.36%, including all electrical noise that was present. However, the majority of this energy is contained below 1 Hz. If the signal was high-passed above 1 Hz, this contribution to the turbulence would be lost. Perhaps, frequencies this low could be considered to have quasi-steady effects. The computed turbulence level, excluding turbulence below 1 Hz, drops to 0.034%. It is currently unclear which number is significant (0.36% or 0.034%), and thus, both numbers are presented.

Spectra at other Reynolds numbers are similar to that in Figure 2 (see Reference 7 for the complete set of spectra). The unfiltered turbulence levels at various Reynolds numbers are: 3.0 $\times 10^5$, 0.17%; 2.0 $\times 10^5$, 0.188%; 1.0 $\times 10^5$, 0.358%; and 0.6 $\times 10^5$, 0.563%. If the contribution to these levels from frequencies below 1 Hz is excluded, the turbulence levels then become: 3.0 $\times 10^5$, 0.0077%; 2.0 $\times 10^5$, 0.0174%; 1.0 $\times 10^5$, 0.064%; and 0.6 $\times 10^5$, 0.050%.

2.2 Wind Tunnel Models

In selecting the model size to obtain the desired Reynolds number, several tradeoffs were considered. To achieve a given test Reynolds number, the measured forces increase with decreasing chord. While large forces are desirable, models with small chords are difficult to build accurately. For this work, a model shop was not used; rather, experienced model sailplane enthusiasts were solicited to build the models. Consequently, construction tolerances were on the order of that found on model sailplanes. A 12 in chord was selected as a compromise between the two competing effects. The model span was 33 3/8 in. Construction techniques ranged from an all-balsa construction with ribs and spars, to fiberglass-covered foam.

As a check for model accuracy and for later computations, every model was profiled using a digitizer to obtain the actual airfoil shape. A comparison was then made with the desired airfoil shape to determine the accuracy of the model. A plot of the error normal to the chord line for the E205 is shown in Figure 3. The error is only determined

for points that were digitized and the best fit between the airfoils was determined using a least squares method developed by Fraser[9]. The root mean square (RMS) of this error ranged from 0.004 in. (0.03%) to 0.035 in. (0.29%) for the 62 models tested, with a median of 0.01 in. (0.08%). For a more complete discussion concerning the accuracy of the models and the actual model coordinates, see Reference 7.

2.3 Measurement Technique and Instrumentation

Lift was measured directly using a mechanical force balance; whereas, drag was found indirectly using the momentum method[10]. Rather than computing the drag based on just one vertical survey, the wake was surveyed and drag was computed at four spanwise locations and then averaged. Measurement of lift will be discussed first.

A sketch of the apparatus to measure lift is shown in Figure 4. The airfoil model was mounted horizontally in the tunnel between two 0.375 in thick Plexiglas end plates (not shown for clarity) to isolate the model ends from the tunnel side-wall boundary layers and the support hardware shown. One side pivoted and the other was free to move vertically on a precison-ground shaft. Two linear ball bearings spaced 8 in apart provided essentially frictionless movement for a carriage (see Figure 4) which held the airfoil and angle of attack control hardware. Spherical bearings were used to minimize moments transmitted to each linear bearing. A force transducer coupled to the carriage through a pushrod sensed the lift (actually 1/2 of the lift was transmitted to the transducer).

The lift force balance consists of a torque motor, lever arm, angular position sensor (angular transformer), and associated control electronics. This device operates by sensing the angular position and feeding an error signal back to the torque motor to keep the angular position fixed. The motor current is linearly related to the torque and thus the device provided excellent linearity. Nine-point calibrations of the force balance were performed frequently to minimize the effects of drift. The overall system had an accuracy of $\pm 0.25\%$ of full scale or ± 0.002 lb_f, whichever is larger. The term full scale refers to the maximum force experienced over a given run at constant Re.

The drag was measured using the momentum method rather than a mechanical force balance which is both difficult and expensive. In addition, if drag is obtained by mechanical means it includes three-dimensional effects due to the side walls. These effects can be reduced by using a three-piece model with only the central panel connected to the force balance. In this case, the angle of attack of the two tips must be kept equal to that of the central portion and the gaps must be minimized. Althaus[11] investigated the effect of a gap on the drag and found that with a 0.5 mm (0.3%) gap and 250 mm (1.56 chord) span, the drag was increased 12% at an α of 9°.

To compute drag using the momentum method, a pitot probe was surveyed through the wake 1.25 chord lengths downstream of the trailing edge to find the velocity deficit. Based on the application of the two-dimensional momentum and continuity equations to a control volume about the airfoil[10], the drag force can be found as:

$$D = b\rho \int_{-\infty}^{\infty} u(U_\infty - u)dy \ , \tag{1}$$

where the integral is performed perpendicular to the freestream, downstream of the airfoil. The freestream velocity is U_∞, y is in the direction normal to the freestream, u is the x-component of velocity at the downstream location, and b is the airfoil span. A typical survey through the wake took 2 minutes, which effectively yielded a time-averaged drag value for each spanwise station. This method of determining the drag is valid only if the wake survey is made at a region where the static pressure is equal to that in the freestream. Wake static pressures at the survey location were found to be very nearly constant.

For pitot probe misalignments of less than 10° the measured total pressure is essentially independent of flow angle. The drag calculation requires only the streamwise component of the velocity and thus transverse velocity components at the survey location can decrease the measured drag. Drag values were found to remain constant as the survey location was moved farther downstream, indicating that the chosen location was sufficiently far from the trailing edge so that transverse velocity components were negligible.

Drag was actually calculated by measuring the difference between the total pressure upstream of the airfoil and that in the wake. Equation (1) may be rewritten to give:

$$D = 2b \int_{-\infty}^{\infty} \sqrt{P_{d\infty} - \Delta P_0}(\sqrt{P_{d\infty}} - \sqrt{P_{d\infty} - \Delta P_0})dy \ , \tag{2}$$

where $P_{d\infty}$ is the freestream dynamic pressure and ΔP_0 is the difference between the total pressure in the freestream and the total pressure in the wake. This pressure difference is small and difficult to measure, requiring a sensitive transducer. A unit made by MKS was used for this purpose with a full scale of 1 mm of Hg and an accuracy of 0.15% of reading. It was factory calibrated against a standard traceable to the National Bureau of Standards.

The spanwise non-uniformity in the wake is well known[11,1]. The drag variation can be on the order of 50% or more at the lower Reynolds numbers, and thus several stations were averaged to provide a more realistic measure of the airfoil performance. As mentioned previously, four spanwise stations were used, spaced uniformly over the central 1 ft of the airfoil.

Wind tunnel corrections[10] were applied to values of C_l and C_d and were approximately 4% and 2% respectively. Error estimates indicate that the accuracy of the resulting C_l value is ±1% and that of the C_d value is ±2%.

The angle of attack of the airfoil was controlled using a gear motor with a worm drive and a sector gear and sensed using an angular transformer, shown in Figure 4, similar to that used in the force balance. The accuracy in determining α was ±0.25°.

All transducer voltages were recorded using a Scientific Solutions A/D interfaced to an IBM PC. The PC controlled the wake pitot probe and airfoil angle of attack. After manually setting the tunnel speed to achieve the desired Reynolds number, the data taking was completely automated and proceeded as follows. The first angle of attack was set, and the location of the wake was found. Next, the four wake surveys were performed, and the angle of attack was increased. Usually, a polar at a given Reynolds number consisted of between 15 and 20 angles of attack from −3° to 15°. This process continued until stall and took typically 1.7 hours. The drag was only measured for

increasing angles of attack, in which case hysteresis was not examined. This was done for two reasons. First, the amount of run time would have been doubled to 3.4 hours on average. Second, hysteresis is a sign of gross laminar separation — a high drag condition. Interest in this investigation was on examining the characteristics of low drag airfoils in application to RC sailplanes. Hence, high drag conditions were of little interest.

In addition to taking lift and drag data simultaneously, which was relatively slow, in many cases a second run was made in which just lift was measured, allowing the angle of attack to be incremented relatively rapidly. In this mode of operation, α was increased up to a pre-set value and then decreased. Hysteresis loops present in the lift behavior were then observed[7]. Approximately 40 angles of attack were used and this process usually required 5 minutes — much less than the 3.4 hours required to obtain a complete drag polar.

2.4 Comparison with Other Facilities

Measurements in other facilities provide a basis of comparison for the lift and drag obtained in this study. Figures 5 *(a–c)* show drag polars obtained in the Princeton tunnel and those in the Delft University tunnel[12] and in the Model Wind Tunnel at the University of Stuttgart[13] for the E205 at Reynolds numbers of 0.6 $\times 10^5$, 1.0 $\times 10^5$, and 2.0 $\times 10^5$. At 2.0 $\times 10^5$all three facilities agree to within 10% over the central region of the lift range. The agreement between Delft and Princeton data at 1.0 $\times 10^5$is also favorable. However, at 0.6 $\times 10^5$, the agreement becomes worse. The discrepancies present are primarily due to differences in (1) flow quality, (2) accuracy of measurements, and (3) methods of measurement. In light of the these important differences, the overall agreement is reasonably good between the three facilities. The remainder of this paper will discuss the results.

3. Discussion of Results

There are several characteristics of an airfoil which can be changed to affect its performance. For example, the contour of the upper and lower surfaces can be altered, boundary layer trips can be added, the trailing edge may be thickened etc. Boundary layer trips are used to reduce the extent of the laminar separation bubble by causing the boundary layer to become turbulent earlier than in the untripped case. However, there is a tradeoff between the drag reduction due to the smaller bubble and the drag increase caused by the presence of the trip as well as the longer region of turbulent flow. Airfoil shape and boundary layer trips as a means of improving performance have been considered and the following sections discuss some of the more important results of this study. For a more complete discussion of all of the results, see Reference 7. First, the airfoil shape is discussed, followed by an illustration of the effects of trips, model accuracy, and finally, the effects of trailing edge thickness.

3.1 Airfoil Design

Three main tools were used to design new airfoils: the Eppler and Somers design code[4], the ISES code written by Drela and Giles[5,6], and the wind tunnel described

above. The Eppler and Somers code formulates the design problem in such a way which allows quick and easy manipulation of the airfoil shape. With a minimum number of parameters, almost any desired velocity distribution can be obtained. However, this code does not accurately predict the performance of airfoils in the Reynolds number range considered here. The Eppler and Somers code was used mainly to obtain the inviscid velocity distributions and to give an estimate of the transition point behavior.

The ISES code solves the two-dimensional Euler equations coupled with a momentum integral boundary layer formulation using a global Newton method. Over the Reynolds number range considered in this investigation it predicts airfoil performance more accurately than the Eppler and Somers code. In particular, the agreement with the experiment at Reynolds numbers of $2.0 \times 10^5$and greater is surprisingly good. However, the agreement depends heavily on the choice of the n value used in the e^n transition criterion. While the ISES code provides a relatively good estimate of the performance, wind tunnel results are the ultimate test of an airfoil.

The design approach was to generate an airfoil with the desired inviscid velocity distribution using the Eppler and Somers code and then predict the performance at a Reynolds number of 2.0×10^5using the ISES code. If the performance was poor, the new airfoil was redesigned and the process repeated. Upon reaching a suitable design through this iteration process, a wind tunnel model was subsequently built and tested. Based upon the wind tunnel results, the new airfoils were further refined and the process repeated.

Before discussing airfoil design, it should be pointed out that for a given chord, wing loading and atmospheric conditions, the relation between C_l and chord Reynolds number is

$$Re \propto \frac{1}{\sqrt{C_l}} .$$

This relation emphasizes the fact that the drag should be minimized for a value of C_l at a given Reynolds number, and this Reynolds number depends on the value of C_l. Thus, the optimum airfoil design is clearly dependent upon the configuration and desired tasks of the aircraft for which it is designed. The designs discussed below were based upon RC sailplane configurations; however, the general conclusions apply to any type of low-Reynolds number aircraft.

A popular RC soaring cross-country airfoil is the Eppler 374. It is commonly used on aircraft intended for high speeds, with little importance placed on the performance at low speeds. The experimentally determined drag polars for this airfoil are shown in Figure 6. This airfoil works well at high speeds because of the small values of the drag coefficient at the higher Reynolds numbers throughout a range of low C_l values. At lower Reynolds numbers, the drag increases dramatically as C_l moves from 0.0 to 0.5, and then decreases again from 0.5 to 0.8. This behavior indicates the formation of a large laminar separation bubble on the upper surface.

The inviscid velocity distribution about the E374 (as predicted by the Eppler and Somers code) for a angle of attack of 5° (with respect to the zero-lift angle of attack) is shown in Figure 7. A "kink" in the upper surface velocity distribution beginning at 40% separates it into two distinct region. Over the first 40% of the upper surface, the velocity changes little, and the majority of recovery takes place over the latter 50% with a relatively strong adverse pressure gradient. At low Reynolds numbers,

this strong adverse pressure gradient results in a large laminar separation bubble. To reduce the drag, the strength of the adverse pressure gradient should be reduced. If the same pressure differential is to be recovered, then the recovery region must start farther upstream, as shown by the dashed line in Figure 7. This longer region of smaller adverse pressure gradient is termed a "bubble ramp." Before this point is discussed further, it is important to observe the behavior of the transition point on the upper surface with increasing C_l.

As a result of the kink in the velocity distribution at 40% chord, the transition point moves rapidly forward with C_l as shown in Figure 8. Of course, transition does not occur at a point but rather over some finite distance. In this case the point refers to the location at which transition was predicted to occur by the Eppler and Somers code using a method based on the shape factor. Knowledge of the shape of the transition point curve is helpful when designing with the Eppler and Somers code because it is similar to the distribution of the design parameter, α^*. (The airfoil design is specified with α^* and ν^4, where α^* is the angle of attack at which the velocity is constant on the surface of the airfoil at a given value of ν, where ν is related the distance along the surface of the airfoil.)

The kink in the velocity distribution was removed by deriving a smooth α^* distribution to define a new airfoil, the SD6060 (see Table 1). The resulting transition point behavior and velocity distribution are shown by the dashed lines in Figures 8 and 7, respectively. Removing the kink shifted the transition point farther forward for C_l greater than 0.5. In this case, separation will occur earlier because of the steeper initial gradient, but, with the transition point farther forward, the separation bubble will be shorter and the drag will be lower. A comparison between the experimentally determined drag polars for the E374 and SD6060 is shown in Figure 9. There has been a reduction in drag throughout the central portion of the polars for all Reynolds numbers, thus, the bubble ramp has reduced the length of the separation bubble. Some of this reduction in drag is due to a thinning of the airfoil; however, the E374 is 10.9% thick and the SD6060 is 10.4% thick so this effect is small. In addition, the increase in drag as C_l approaches 1.0 is more gradual in the case of the SD6060, which is consistent with the more smooth forward movement of the transition point.

A further example illustrating the effectiveness of a bubble ramp in the upper surface velocity distributions can be seen by comparing the E205 and the S3021[14]. The E205 is usually used as a "multi-task" airfoil because of its relatively good performance at both high and low lift. This airfoil has an upper-surface velocity distribution which is similar to the E374 in that it also contains a kink. The velocity distribution of the S3021 is essentially the same as that of the E205 except the kink has been replaced with a bubble ramp as in the SD6060. Figure 10 shows a comparison between the drag polars of the E205 and S3021 at several Reynolds numbers. The differences are similar to those noted between the E374 and SD6060. At all Reynolds numbers, the drag of the S3021 is lower than that of the E205 in the central region of the polars. However, at the highest Reynolds number, 3.0×10^5, the E205 has lower drag than the S3021 for $C_l = 0.9$. As discussed earlier, as the speed increases, the lift coefficient decreases so that, for typical low Reynolds number configurations, at a Reynolds number of 3.0×10^5, the lift coefficient would be considerably less than 0.9. Thus, for low Reynolds number aircraft, the S3021 will perform better than the E205. Further examples of performance

improvements by the use of bubble ramps are given in Reference 7. These examples illustrate improvements, but the optimum bubble ramp shape and location remains to be determined.

3.2 Boundary Layer Trips

In the last section, altering the shape of the upper surface to reduce the size of the laminar separation bubble was discussed. This section deals with an alternate method, the use of boundary layer turbulators or trips. Throughout this investigation, several different types of trips were used on a variety of airfoils at different locations. Only a few of them will be discussed here.

Two-dimensional trips were made from automobile pin-striping tape placed along the span at a constant chord location. A trip height of 0.17% chord was found to be close to an optimum in terms of its ability to promote transition at low Reynolds numbers and not cause excessive drag at high Reynolds numbers. The typical effect of such a trip was to decrease the drag at Reynolds numbers below about $1.5 \times 10^5$and increase the drag at higher Reynolds numbers. Of course these trends are for the particular class of airfoils tested. Most of the airfoils were on the order of 10% thick and had approximately 2.5% camber. An example of the use of trips is shown in Figure 11 which depicts drag polars of the E374 with and without a boundary layer trip at two Reynolds numbers. In this case, the trip was placed at 20% chord and is 1.0% wide. Note that the drag at $1.5 \times 10^5$is decreased by the presence of the trip while the drag at $3.0 \times 10^5$is increased. Similar behavior was seen in the case of many other airfoils[7]. It was also found that using trips on airfoils which already had low drag at low Reynolds numbers yielded a smaller benefit. For example, boundary layer trips improved the performance of the E374 by a greater amount than for the SD6060.

Zig-zag tape, as used on full-scale sailplanes, was also investigated as a means of tripping the boundary layer. Based upon data on the S4061[7,14], there was no advantage to using the zig-zag tape. While it may be more effective at causing transition[15], the benefit of shortening the laminar separation bubble was balanced by a higher trip drag.

Hemispheres (commonly called upper-surface bumps) with a diameter of 0.15 in (10 viscous units) and a spacing of 0.45 in (100 viscous units at $Re = 2.0 \times 10^5$) were also used to trip the boundary layer. These dimensions correspond to the width and spacing of low-speed streaks observed in transitional and turbulent boundary layers and thus are reasonable choices for the generation of artificial low-speed streaks. Further discussions of this subject can be found in many references, including 16 and 17. The viscous units were calculated based upon the local boundary layer properties at the trip location. Results from the Miley airfoil[18] showed that hemispheres (bumps) were somewhat less effective that the simple two-dimensional trip[7]. Other airfoils exhibited similar trends[7].

In addition to surface protuberances, upper-surface blowing was also used to trip the boundary layer. A hollow model of the HQ2/9 was tested with holes drilled normal to the surface across the span at 50% chord and spaced at approximately 100 viscous units (0.45 in at $Re = 2.0 \times 10^5$). (The designation "HQ"is for H. Quabeck — not to be confused with airfoils designed by K. H. Horstmann and A. Quast.) A ram inlet pressurized the airfoil to feed the blowing holes. Comparisons with a two-dimensional

trip at the same location indicated that the blowing was less effective in reducing drag, not considering the drag of the ram inlet.

It is clear from this work that an airfoil which performs poorly at low Reynolds numbers can be improved through the use of trips. This will often degrade the performance at higher Reynolds numbers however. The choice of trip appears to be the simple two-dimensional strip with a height of 0.17% for the airfoils considered here (approximately 10% thick with 2.5% camber). In this study the location for the trip was chosen based upon both intuition and reason. Using the ISES code, an estimate of the separation point at a given angle of attack could be found. The distance upstream of this point necessary for a trip to prevent separation was generally chosen, rather arbitrarily, as 5–10% of the chord. This method appeared to work reasonably well. However, this distance is certainly a function of Reynolds number, trip type and size. The current inability to predict the transitional flows near a trip and near separation indicate that trip location may be best guided by experiment. More importantly, the question: "Should the optimum airfoil for a given task make use of trips?", has not yet been answered.

3.3 Effects of Contour Inaccuracies

Often when constructing an airfoil, an estimate of the accuracy required to achieve the expected performance is necessary. In the current study, two models of a given airfoil were tested in several cases, allowing the effect of accuracy and surface finish to be examined.

Two models of the E205, E214, E374, E387, S3021, S4061, and SD7032 were tested. For a given airfoil, differences between the models were compared to differences in the resulting performance. None of the models had surface discontinuities so that all errors were distributed over some chordwise distance. The correlation between accuracy and performance is difficult to make; however, the following observations were made. First, if the error in surface contour is greater than 0.2% of chord, the performance will be affected. Differences in the trailing edge included angle seemed to have little effect in comparison to other errors. The two E205 models performed the most alike and had upper surfaces which were quite similar from 10% to 60% of chord. Further conclusions are difficult to draw, but it may be assumed that errors in the region where a separation bubble forms will have the largest effect on performance. Additional details can be found in Reference 7.

It is often believed that the accuracy near the leading edge is quite important[13]. Modeling clay was applied to the first 15% of the upper surface of the E374 in an irregular pattern to investigate this claim. The clay was roughly 0.2% chord thick and extended over the entire span of the model. Although the clay was wavy, all edges were carefully blended to the surface. In comparison with the clean E374 data, there was almost no difference at Reynolds numbers of 1.5×10^5 and above. At $Re = 1.0 \times 10^5$ there was a slight decrease in the drag peak near $C_l = 0.5$, which was probably due to an enhancement of transition causing the bubble to become shorter.

A common error when constructing airfoils is a thick trailing edge. The adverse effects of such an error were investigated on the DAE51, the airfoil used on the propeller of the Daedalus human powered aircraft[19] This airfoil was first tested as originally

constructed, and then the trailing edge was thickened by 0.8%. The thickness was fared into the original contour over the latter 14% of the upper surface. A comparison between the drag polars of the DAE51 with and without the modification are shown in Figure 12 for three Reynolds numbers. The drag is clearly increased for the higher Reynolds numbers, but at a Re of 1.0 $\times 10^5$there is little difference. At this Reynolds number, the flow is probably separated at the trailing edge so the thickness has little effect. This increased drag is in agreement with Althaus[20] who found similar results for thickened trailing edges. Therefore, under most conditions, a thin trailing edge is desirable.

4. Conclusions

Several airfoils were tested in efforts to design new and improved airfoils. Two methods to reduce the drag of an airfoil operating at low Reynolds numbers were examined. First, a long region of roughly constant adverse pressure gradient on the upper surface (termed a bubble ramp) achieved a lower drag than the more conventional laminar flow-type velocity distribution in which the pressure remains approximately constant initially, and then more rapidly recovers. Second, trips were used to reduce drag by shortening the laminar separation bubble. Several different methods of tripping the boundary layer were investigated. A simple two-dimensional trip performed as well or better than zig-zag tape used on full-size sailplanes, hemispheres (bumps) attached to the surface, and blowing normal to the surface. Boundary layer trips were less effective at improving airfoils which normally had low drag. The question still remains whether the optimum airfoil for a given task requires boundary layer trips or simply an efficient shape, possibly similar to the bubble ramp.

During the course of this work, the effects of geometrical errors were also observed. As a general guideline, accuracy should be held to within 0.2% of chord, with particular attention paid to the region from 20% to 60% on the upper surface where laminar separation bubbles will form. Accuracy at the leading edge is not as critical. Finally, trailing edges should be thin for low drag.

Acknowledgments

This was a privately funded program that could not have been performed without the encouragement, support, and guidance of several individuals. The authors gratefully acknowledge the support and expertise of David Fraser, President, Fraser Volpe Corp., without whom the scale of this work would have been an order of magnitude smaller. Special thanks go to Prof. A. J. Smits at the Princeton University Gas Dynamics Laboratory. Also Prof. Lam and Prof. Curtiss at Princeton are thanked for their support. Thanks are expressed to Prof. M. D. Maughmer at Penn State for his helpful discussions during the course of the work. All of the models tested during this program were made by RC sailplane enthusiasts, and their combined efforts are greatly appreciated. Finally, MKS and Scientific Solutions, Inc. are gratefully acknowledged for their donations of instrumentation.

References

[1] van Ingen, J. L. and Boermans, L. M. M., "Aerodynamics at Low Reynolds Numbers: A Review of Theoretical and Experimental Research at Delft University of Technology," Aerodynamics at Low Reynolds Numbers $10^4 < Re < 10^6$ International Conference, London, October 1986.

[2] Dobbinga, E., van Ingen, J. L., and Kooi, J. W., "Some Research on Two-Dimensional Laminar Separation Bubbles," AGARD CP-102, Paper 2, Lisbon, 1972.

[3] Eppler, R. and Somers, D. M., "Airfoil Design for Reynolds Numbers Between 50,000 and 500,000," Proceedings of the Conference on Low Reynolds Number Airfoil Aerodynamics, Notre Dame, Indiana, June 1986.

[4] Eppler, R. and Somers, D. M., "A Computer Program for the Design and Analysis of Low-Speed Airfoils, Including Transition," NASA TM 80210, August 1980.

[5] Drela, M. and Giles, M. B., "Viscous-Inviscid Analysis of Transonic and Low-Reynolds Number Airfoils," AIAA J., Vol. 25, No. 9, September 1987.

[6] Drela, M. and Giles, M. B., "ISES: A Two-Dimensional Viscous Aerodynamic Design and Analysis Code," AIAA Paper 87-0424, January 1987.

[7] Selig, M. S., Donovan, J. F., and Fraser, D., Airfoils at Low Speeds, Soartech #8, published by H. A. Stokely, 1504 North Horseshoe Circle, Virginia Beach, VA, 23451, U.S.A., July 1989.

[8] Perry, A. E., Hot-Wire Anemometry, Oxford University Press, 1982.

[9] Fraser, D.B., private communications, 1989.

[10] Rae, H. and Pope, A., Low-Speed Wind Tunnel Testing, John Wiley & Sons, second ed., 1984.

[11] Althaus, D., "Recent Wind Tunnel Experiments at Low Reynolds Numbers," Aerodynamics at Low Reynolds Numbers $10^4 < Re < 10^6$ International Conference, London, October 1986.

[12] Volkers, D. F., "Preliminary Results of Wind Tunnel Measurements on Some Airfoil Sections at Reynolds Numbers between 0.6×10^5 and 5.0×10^5," Memo M-276, Delft University of Technology, The Netherlands, 1977.

[13] Althaus, D., Profilpolaren für den Modellflug, Necker-Verlag, Villengen-Schennigen, University of Stuttgart, FRG, 1980.

[14] Selig, M. S., The Design of Airfoils at Low Reynolds Numbers, Soartech #3, published by H. A. Stokely, 1504 North Horseshoe Circle, Virginia Beach, VA, 23451, U.S.A., July 1984. Also AIAA-85-0074.

[15] Hegarty, J. L. and Hama, F. R., "Further Investigation on the Trianglar-Pattern Stimulator," University of Maryland, TN-107, AFOSR TN-57-616, 1957.

[16] Hama, F. R. "An Efficient Tripping Device," Journal of the Aeronautical Sciences, (Readers' Forum), Vol. 24, No. 3, pp 236-237.

[17] Schlichting, H., Boundary-Layer Theory, McGraw-Hill, 1979.

[18] Miley, S. J., "On the Design of Airfoils for Low Reynolds Numbers," AIAA Paper 74-1017, September 1974.

[19] Drela, M., "Low-Reynolds-Number Airfoil Design for the M.I.T. Daedalus Prototype: A Case Study," AIAA J., Vol. 25, No. 8, August 1988.

[20] Althaus, D., "Effects on the Polar Due to Changes or Disturbances to the Contour of the Wing Profile," Technical Soaring, Vol. 10, No. 1, January 1986.

Table 1. - SD6060 Airfoil Coordinates

1	1.00000	0.00000	17	0.43386	0.06866	33	0.00495	−.00647	49	0.62223	−.02527
2	0.99661	0.00023	18	0.38566	0.07003	34	0.01525	−.01148	50	0.67254	−.02231
3	0.98660	0.00108	19	0.33862	0.07020	35	0.03068	−.01612	51	0.72116	−.01906
4	0.97033	0.00283	20	0.29316	0.06922	36	0.05114	−.02025	52	0.76761	−.01568
5	0.94829	0.00559	21	0.24976	0.06715	37	0.07648	−.02381	53	0.81133	−.01236
6	0.92100	0.00941	22	0.20883	0.06402	38	0.10645	−.02678	54	0.85176	−.00922
7	0.88905	0.01419	23	0.17076	0.05988	39	0.14078	−.02919	55	0.88838	−.00638
8	0.85301	0.01977	24	0.13589	0.05480	40	0.17909	−.03105	56	0.92070	−.00399
9	0.81346	0.02595	25	0.10456	0.04887	41	0.22096	−.03238	57	0.94818	−.00214
10	0.77096	0.03248	26	0.07700	0.04218	42	0.26592	−.03321	58	0.97032	−.00090
11	0.72602	0.03912	27	0.05344	0.03486	43	0.31347	−.03354	59	0.98661	−.00024
12	0.67917	0.04563	28	0.03399	0.02710	44	0.36306	−.03338	60	0.99662	−.00002
13	0.63091	0.05177	29	0.01879	0.01913	45	0.41413	−.03273	61	1.00001	0.00000
14	0.58174	0.05738	30	0.00790	0.01132	46	0.46614	−.03159			
15	0.53222	0.06225	31	0.00148	0.00411	47	0.51852	−.02995			
16	0.48283	0.06606	32	0.00025	−.00159	48	0.57073	−.02784			

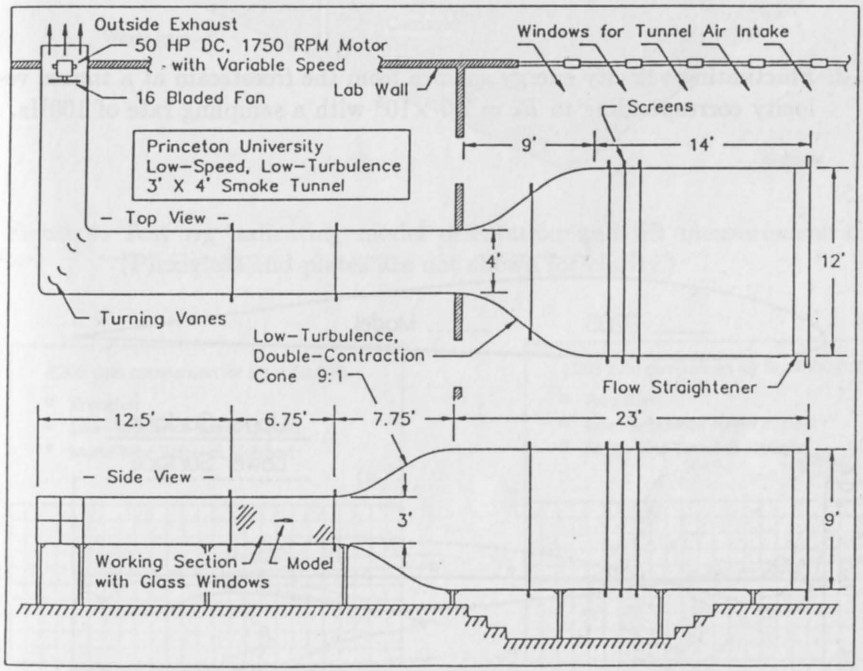

Figure 1. Diagram of the Princeton University low speed wind tunnel (not to scale).

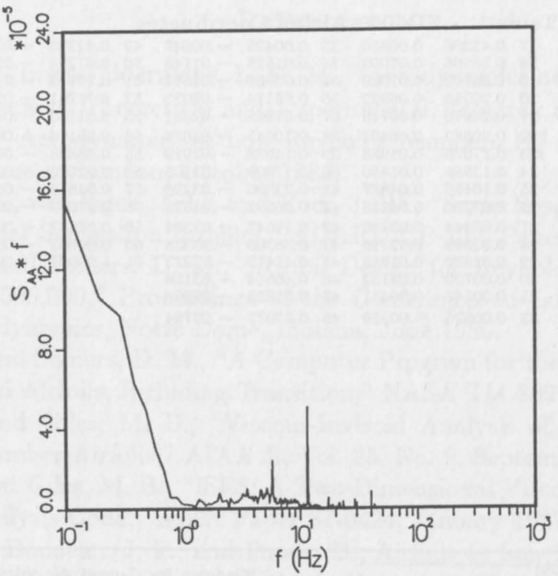

Figure 2. Fluctuating velocity energy spectra from the freestream at a tunnel velocity corresponding to $Re = 1.0 \times 10^5$ with a sampling rate of 100Hz.

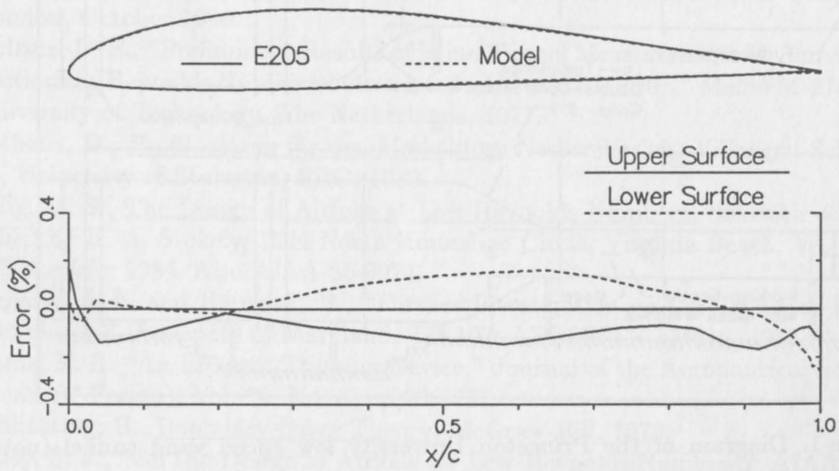

Figure 3. Comparison of the digitized E205 model surface to the desired shape, with the error plotted below as a percentage of the chord.

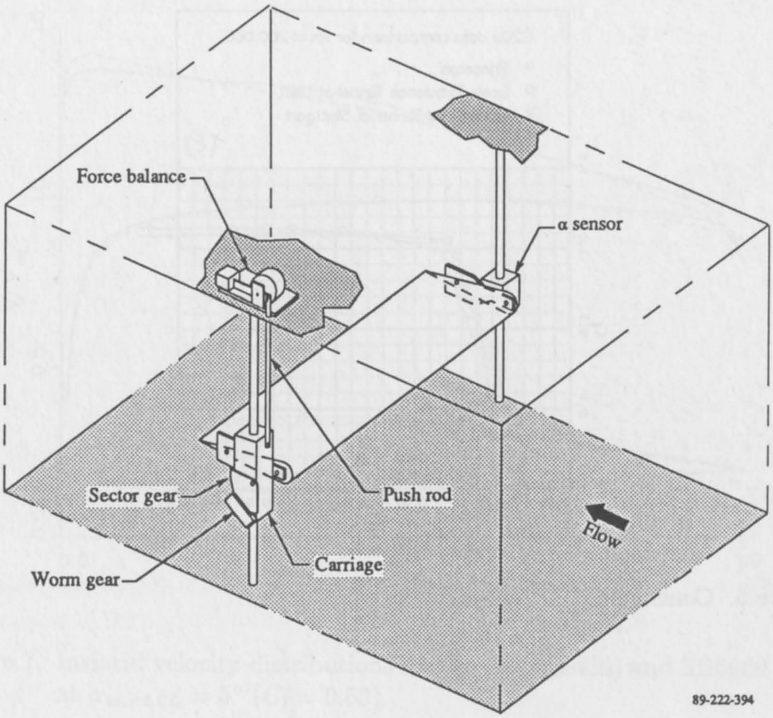

Figure 4. Test rig indicating model orientation and lift measurement method. (Plexiglass end plates are not shown for clarity.)

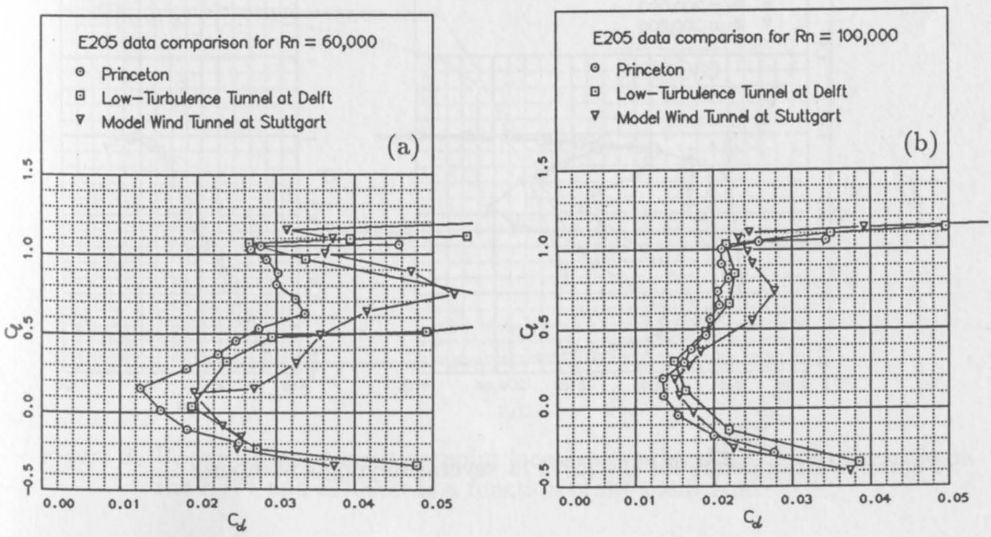

Figure 5. Comparison of the E205 data with that of Delft[12] and Stuttgart[13] at Reynolds numbers of (a) 0.6 $\times 10^5$, (b) 1.0 $\times 10^5$, and (c) 2.0 $\times 10^5$.

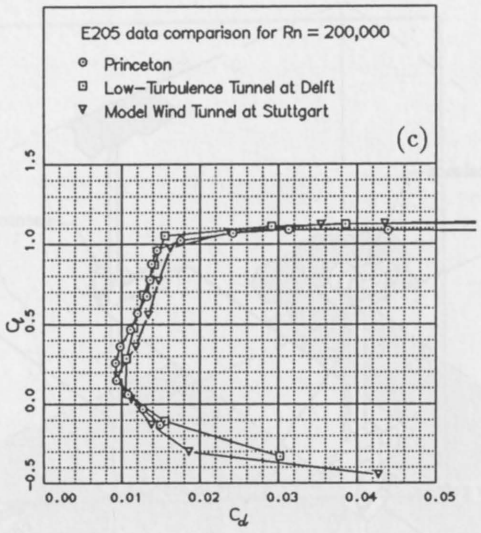

Figure 5. Continued.

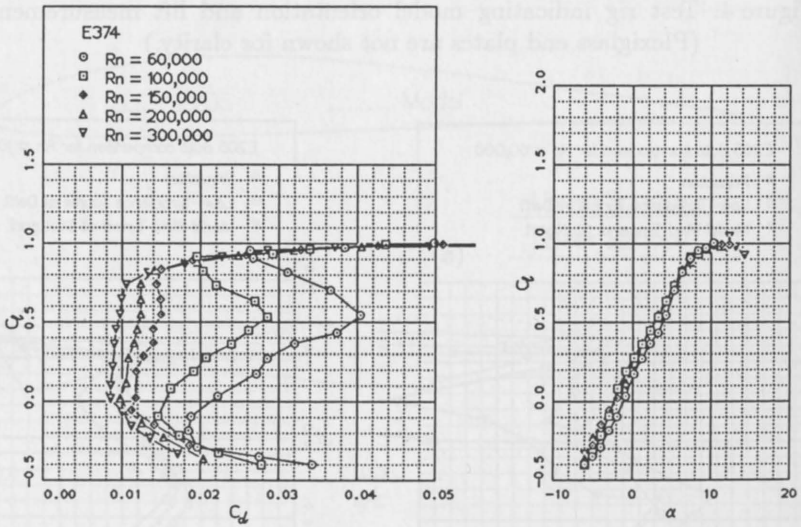

Figure 6. Drag polars for the E374 at several Reynolds numbers.

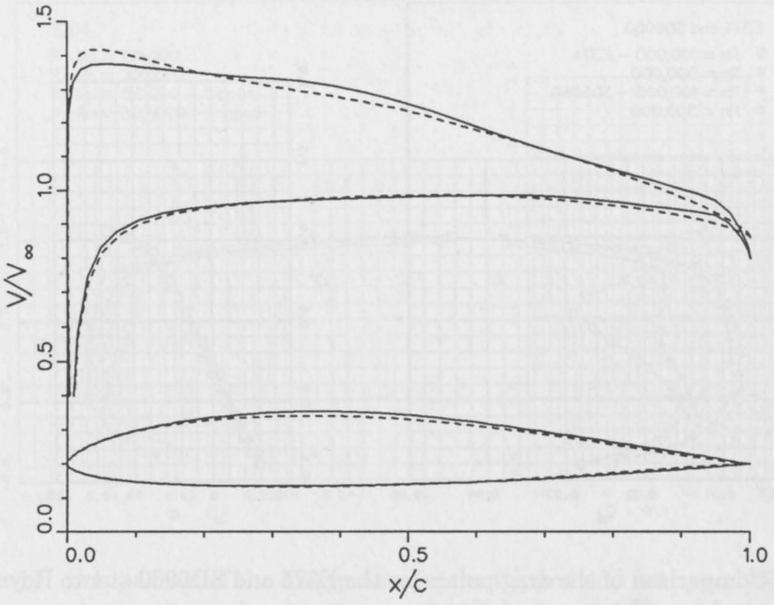

Figure 7. Inviscid velocity distributions for the E374 (solid) and SD6060 (dashed) at $\alpha_{w.r.t.0L} = 5°$ ($C_l = 0.55$).

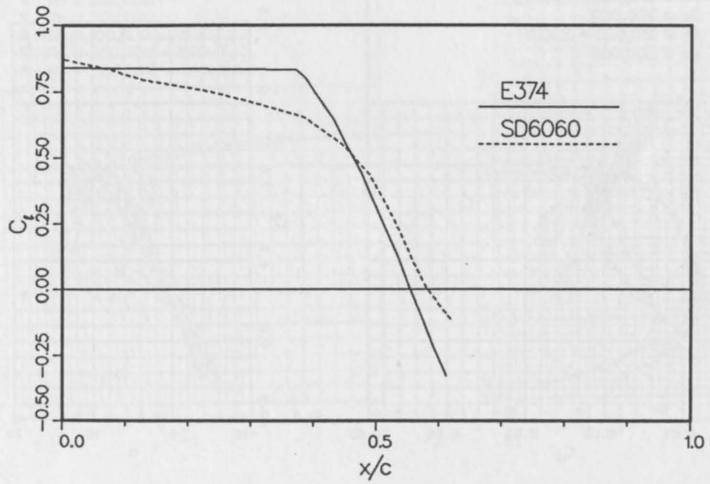

Figure 8. Upper surface transition point location predicted by the Eppler code on the E374 and SD6060 as a function of lift coefficient.

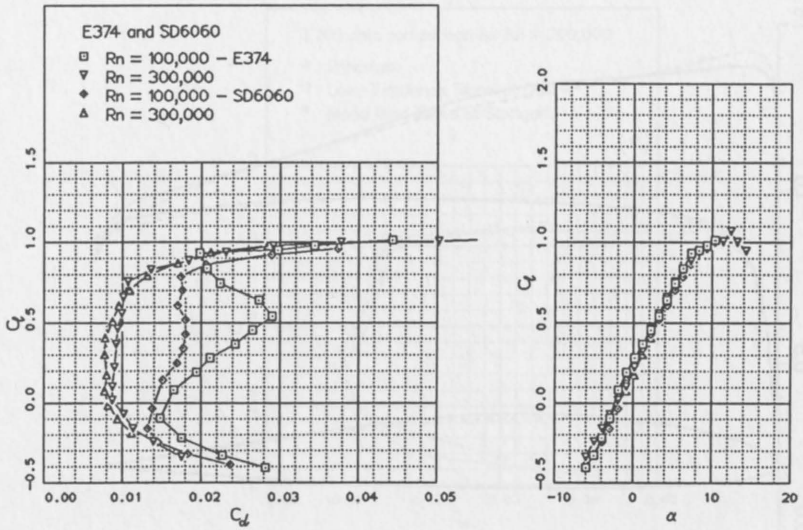

Figure 9. Comparison of the drag polars for the E374 and SD6060 at two Reynolds numbers.

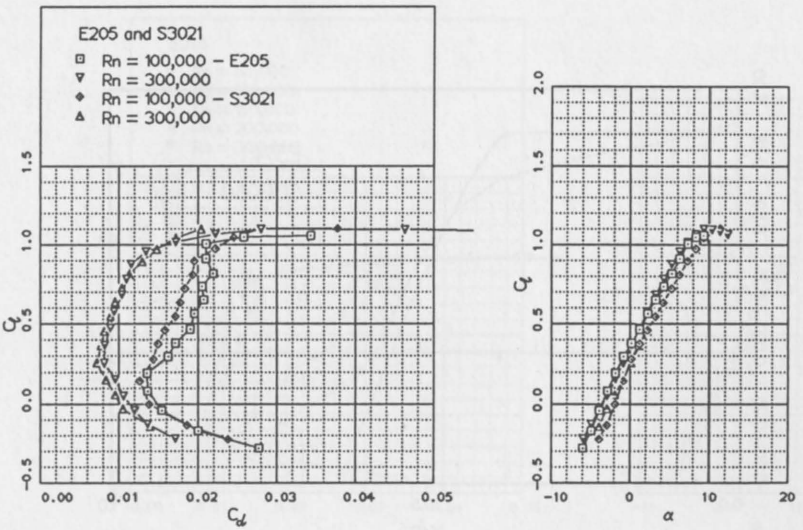

Figure 10. Comparison of the drag polars for the E205 and S3021 at two Reynolds numbers.

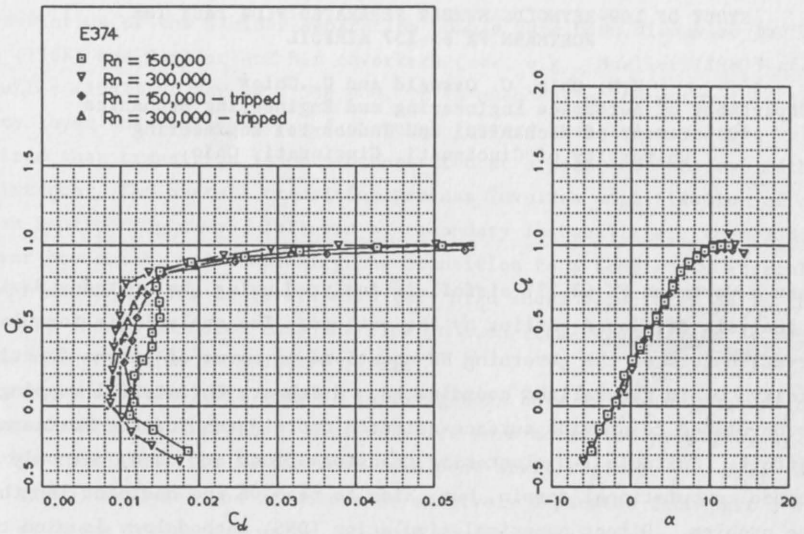

Figure 11. Comparison of the drag polars for the tripped and untripped E374. (simple two-dimensional trip strip: 0.17% high and 1.% wide)

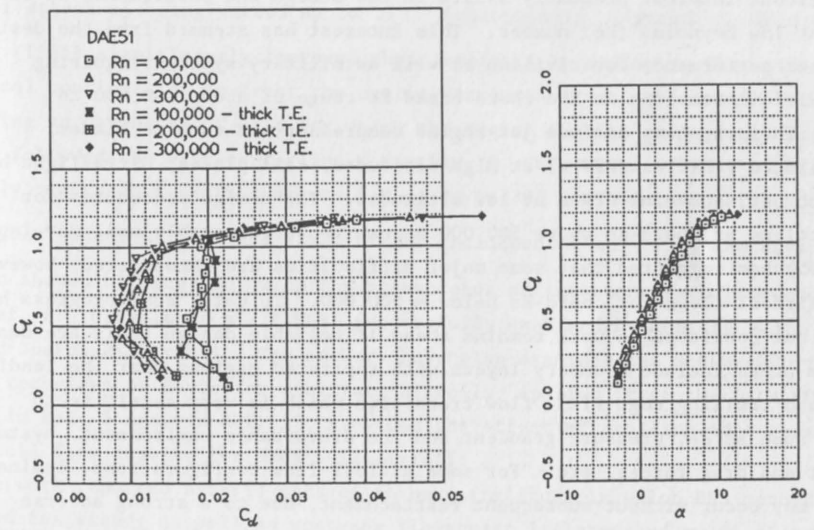

Figure 12. Drag polars of the DAE51 with and without a thickened trailing edge.